Article

Current Biology

Theta Oscillations in the Human Medial Temporal Lobe during Real-World Ambulatory Movement

Highlights

- Movement-related 8 Hz theta oscillations occur in the human medial temporal lobe
- Theta occurs in short bouts that are more prevalent during fast versus slow movements
- The duration and prevalence of theta are higher in a congenitally blind participant
- Combined motion capture and iEEG allow for future studies of ambulatory behavior

Authors

Zahra M. Aghajan, Peter Schuette, Tony A. Fields, ..., John Stern, Itzhak Fried, Nanthia Suthana

Correspondence

nsuthana@mednet.ucla.edu

In Brief

Aghajan et al. record deep brain activity, during untethered freely moving behavior, from participants chronically implanted with depth electrodes. They demonstrate that 8 Hz theta oscillations, the hallmark of spatial navigation in rodents, also occur in humans, albeit in shorter bouts that are more prevalent during fast versus slow movements.

M. Aghajan et al., 2017, Current Biology *27*, 3743–3751
December 18, 2017 Published by Elsevier Ltd.
https://doi.org/10.1016/j.cub.2017.10.062

Current Biology
Article

Theta Oscillations in the Human Medial Temporal Lobe during Real-World Ambulatory Movement

Zahra M. Aghajan,[1] Peter Schuette,[1] Tony A. Fields,[2] Michelle E. Tran,[3] Sameed M. Siddiqui,[1] Nicholas R. Hasulak,[4] Thomas K. Tcheng,[4] Dawn Eliashiv,[2] Emily A. Mankin,[3] John Stern,[2] Itzhak Fried,[1,3,5,6] and Nanthia Suthana[1,3,7,8,*]
[1]Department of Psychiatry and Biobehavioral Sciences, Semel Institute for Neuroscience and Human Behavior, University of California, Los Angeles, Los Angeles, CA 90095, USA
[2]Department of Neurology, University of California, Los Angeles, Los Angeles, CA 90095, USA
[3]Department of Neurosurgery, David Geffen School of Medicine, University of California, Los Angeles, Los Angeles, CA 90095, USA
[4]NeuroPace, Inc., Mountain View, CA 94043, USA
[5]Functional Neurosurgery Unit, Tel Aviv Medical Center, Tel Aviv 64361, Israel
[6]Sackler Faculty of Medicine, Tel Aviv University, Tel Aviv 69978, Israel
[7]Department of Psychology, University of California, Los Angeles, Los Angeles, CA 90095, USA
[8]Lead Contact
*Correspondence: nsuthana@mednet.ucla.edu
https://doi.org/10.1016/j.cub.2017.10.062

SUMMARY

The theta rhythm—a slow (6–12 Hz) oscillatory component of the local field potential—plays a critical role in spatial navigation and memory by coordinating the activity of neuronal ensembles within the medial temporal lobe (MTL). Although theta has been extensively studied in freely moving rodents, its presence in humans has been elusive and primarily investigated in stationary subjects. Here we used a unique clinical opportunity to examine theta within the human MTL during untethered, real-world ambulatory movement. We recorded intracranial electroencephalographic activity from participants chronically implanted with the wireless NeuroPace responsive neurostimulator (RNS) and tracked their motion with sub-millimeter precision. Our data revealed that movement-related theta oscillations indeed exist in humans, such that theta power is significantly higher during movement than immobility. Unlike in rodents, however, theta occurs in short bouts, with average durations of ~400 ms, which are more prevalent during fast versus slow movements. In a rare opportunity to study a congenitally blind participant, we found that both the prevalence and duration of theta bouts were increased relative to the sighted participants. These results provide critical support for conserved neurobiological characteristics of theta oscillations during ambulatory spatial navigation, while highlighting some fundamental differences across species in these oscillations between humans and rodents.

INTRODUCTION

The crucial role of the medial temporal lobe (MTL) in declarative memory and encoding new experiences is unequivocal based on an abundant body of literature in humans and many mammalian species [1–3]. It is posited that the ongoing rhythmic oscillatory activity in the local field potential (LFP) is critical for the temporal organization of neural assemblies in this region, allowing appropriate modification of synaptic connections. Additionally, various frequency bands are thought to be involved in different brain functions [4, 5]. In particular, the 6–12 Hz frequency range—commonly referred to as the theta rhythm—has been associated with exploratory behavior [6, 7] and rapid eye movement (REM) sleep [8], and different features of this rhythm have been linked to memory performance on various tasks [9–13].

In the rodent hippocampus, theta oscillations (6–12 Hz) are most prominent during locomotion, even during tasks with no memory demand, such as running on linear tracks and random foraging, although a lower frequency theta (3–7 Hz) has been reported during periods of immobility [14]. Theta has also been reported in other species, such as cats [15], and in shorter oscillatory bouts in bats [16, 17], non-human primates [18, 19], and humans [20–22]. There is, thus, an apparent discrepancy in the presence of persistent movement-related theta across species. This issue is confounded by the fact that—due to restrictions imposed by recording techniques—electrophysiological recordings in primates, contrary to those performed in rodents, have typically employed virtual navigation in stationary subjects. Recent rodent hippocampal recordings during virtual navigation have demonstrated significant differences in theta dynamics between virtual and real-world navigation, including lower frequencies and a lack of frequency-speed dependence in virtual navigation [23, 24]. In light of these studies, resolving whether persistent movement-related theta could be a feature of human navigation requires directly probing the intracranial electroencephalogram (iEEG) during natural voluntary human movement. Movement-related theta was observed in walking humans in one recent study [22]. However, due to lack of motion tracking, this study did not allow for characterization of theta with respect to movement parameters [22]. We therefore conducted an experiment to elucidate the properties of theta oscillations in the MTL of freely moving humans. This was made possible by using a novel chronic implant that allowed for wireless iEEG recording outside of a restrictive hospital setting.

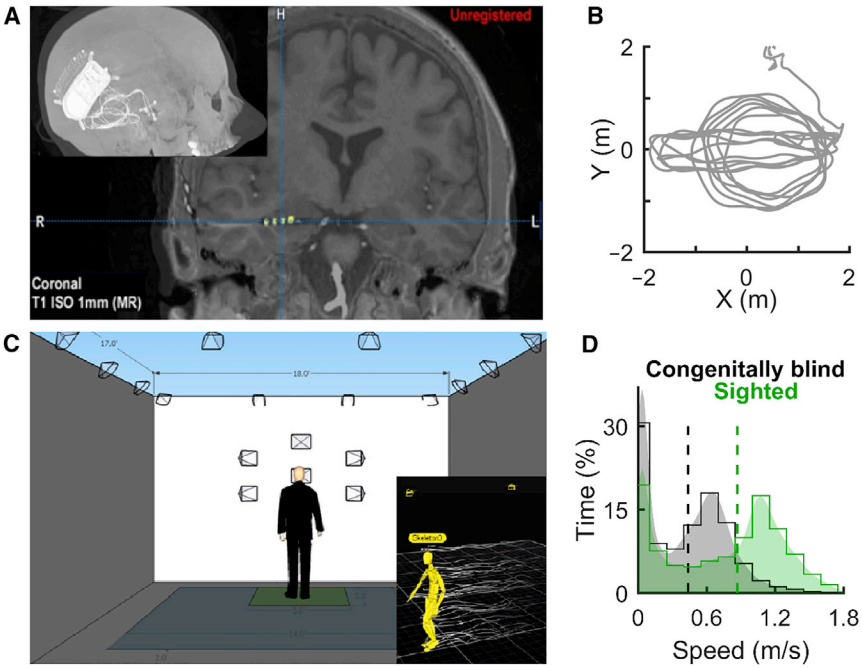

Figure 1. Simultaneous Motion Tracking and iEEG Recording within the Human MTL

(A) Example post-operative CT of a participant with an implanted electrode in the right hippocampus (top left) along with a coronal view of a high-resolution MRI overlaid with co-registered electrodes (shown in yellow).

(B) Sample trajectory of a participant during one complete trial consisting of linear and circular movements.

(C) Schematic of the setup of cameras used for motion capture (see the STAR Methods). Inset: real-time motion tracking of an example participant is shown.

(D) Movement speed distribution of all sighted participants (green; median, [25th, 75th] = 0.87, [0.20, 1.14] m/s, N_{trials} = 21) and one congenitally blind participant (black; median, [25th, 75th] = 0.44, [0.05, 0.68] m/s, N_{trials} = 7). Dashed vertical lines indicate median value; shaded areas correspond to kernel smoothing function estimates of the distributions.

See also Tables S1 and S2 and Movie S1.

RESULTS

MTL Recordings in Freely Walking Humans Implanted with the RNS System

Participants were four neurosurgical patients (one congenitally blind), chronically implanted with the FDA-approved NeuroPace RNS System (responsive neurostimulator) (Figure 1A) for treatment of pharmacologically intractable epilepsy. For participant demographics, see Tables S1 and S2. For studying ambulatory movement, the RNS System provides two significant advantages over traditional recording techniques in the hospital setting: motion and muscle artifacts are entirely eliminated (since the implant is fully shielded); subjects are able to freely move around without the limitations imposed by restrictive hospital equipment, related safety protocols, and tethered implanted wires connected to large recording equipment. The RNS System recorded continuous bipolar iEEG activity from two adjacent electrode contacts (sampling rate: 250 Hz, with an analog filter equivalent to a first-order Butterworth with 3 dB attenuation at the cutoff frequencies (4–90 Hz); for a detailed description, see the STAR Methods). Participants with MTL electrodes performed a task in which they were instructed to walk along linear and circular paths at slow and fast speeds. A complete trial consisted of the following four movements: (1) slow movement in straight lines, (2) slow movement in circles, (3) fast movement in straight lines, and (4) fast movements in circles; the order of these instructions was randomized (Figure 1B; see the STAR Methods). Within each trial, after the participants finished one type of movement, they were temporarily immobile until a pre-recorded voice command informed them to begin the next type of motion.

Motion tracking was performed using the OptiTrack system (Natural Point), which was capable of recording participants' positional and rotational information (Figures 1C and 1D; Movie S1). Position information was recorded simultaneously with iEEG data (Figure 2A; Movies S2 and S3; see the STAR Methods). The locations of electrodes were determined by co-registration of high-resolution post-operative computed tomography (CT) images with high-resolution pre-operative magnetic resonance images that had been subjected to automated segmentation of MTL subregions to facilitate visualization (Figure 2B; Table S3; see the STAR Methods). Although the RNS System is implanted in potential seizure onset zones, pairs of electrode contacts frequently span up to 10 mm of tissue, thereby leading to some recordings in healthy tissue. In the current study, each participant had at least one contact ipsilateral to the seizure onset zone (Table S3). To further account for epileptic tissue in all contact recordings, we eliminated epochs with putative epileptic activity by using a thresholding algorithm, similar to methods previously described [25] (see the STAR Methods and Figure S1A), and visual inspection, which resulted in discarding 3% of the data per trial (median, [25th, 75th] = 3.04%, [1.32%, 4.62%], $N_{participants}$ = 4, $N_{trials \times channels}$ = 112; Figure S1B). Note that the responsive therapy (stimulation feature) was turned off during the experiments and, hence, there was no stimulation artifact in the data (see the STAR Methods).

Theta Oscillations during Movement and Immobility Periods

Examination of raw iEEG traces revealed striking theta oscillations, which were readily visible (Figure 2A; Movies S2 and S3). We first sought to examine whether these theta oscillations were more prominent during movement than immobility and would thus be considered an analog of movement-related theta in rodents. To address this, in each trial a multi-taper power spectrum was calculated within each condition, i.e., movement versus immobility, defined as speeds below 10 cm/s. We found that theta power was indeed higher during movement, as shown in individual examples (Figure 3A; Figure S2). The theta power

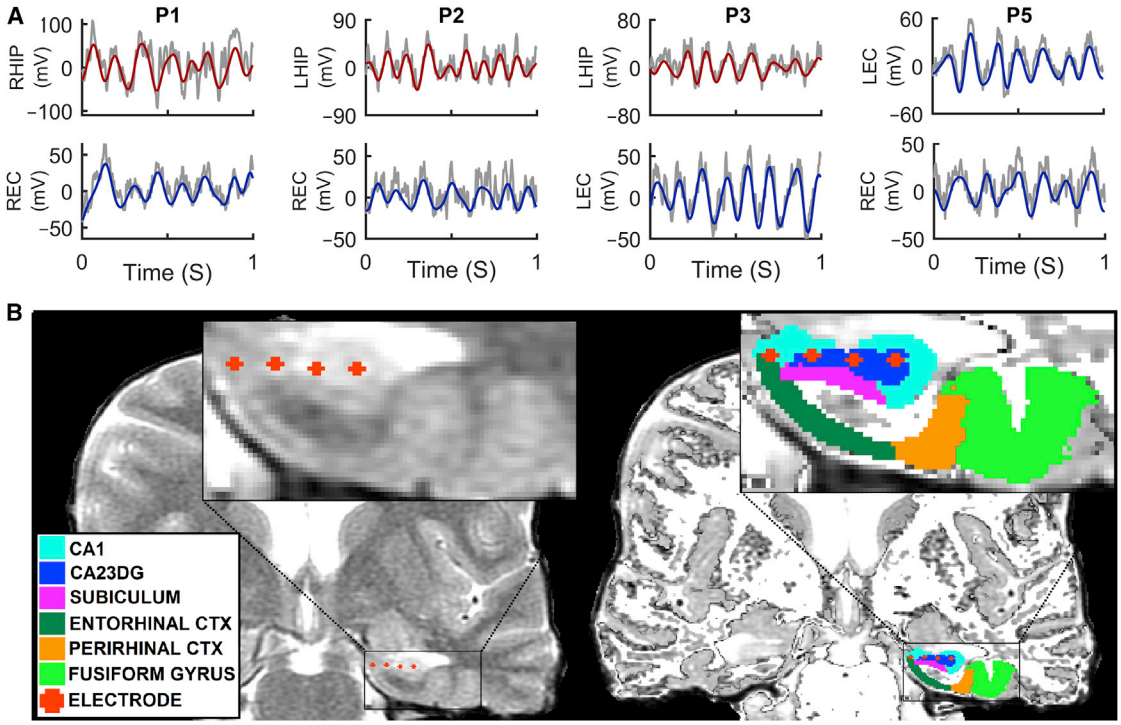

Figure 2. Example Theta Oscillations in the Human MTL

(A) Example 1-s-long raw iEEG traces (gray) from the MTL of all study participants overlaid with filtered (3–12 Hz) theta oscillations (hippocampal and entorhinal theta shown in red and blue, respectively). Participant P3 is congenitally blind. Note that, on average, the duration of theta bouts is shorter than 1 s, as demonstrated in this figure (for a detailed characterization, see Figure 4).

(B) (Left) Sample electrode locations from a participant (P2) overlaid onto coronal pre-operative high-resolution MRI. (Right) Automated MTL subregion segmentation (note that different colors correspond to different areas) demonstrating electrode locations in an example participant. White areas correspond to white matter.

See also Figures S1 and S6, Table S3, and Movies S2 and S3.

index, a normalized measure of power difference between the two conditions, was significantly positive for all participants (Figure 3B; see the STAR Methods) and on the population level (median, [25^{th}, 75^{th}] = 0.40, [0.30, 0.51]; $p = 4.56 \times 10^{-20}$, Wilcoxon signed-rank test; n = 112). This analysis assumes that individual data points are statistically independent and cannot account for potential clustering of the data due to the within-subject repeated-measures design. To address this, since neighboring electrode contacts and repeated trials from the participant do not constitute independent samples, we used generalized estimating equations (GEEs) [26, 27] to model relative theta power as a function of whether the participant was moving or not (see the STAR Methods). In agreement with the results obtained from the theta power index distribution, we found that movement is indeed a significant factor in predicting relative theta power ($p < 0.001$, Wald $\chi^2 = 172.50$; estimated means and 95% Wald confidence intervals are as follows: 0.70, [0.67, 0.73] for movement and 0.30, [0.27, 0.33] for immobility).

Prevalence of Theta Oscillations

To further investigate how movement speed modulated theta, we quantified the prevalence of significant theta oscillations during fast versus slow movements using the better oscillation detection (BOSC) method [28–30]. This method uses wavelets to provide a power estimate for the signal, and—accounting for the background 1/f dependency—it can detect periods with significant oscillations at different frequencies that exceed thresholds for power and duration (see the STAR Methods). This method was recently used by Watrous et al. [31] in a comparative study of theta oscillations between virtual navigation studies in humans and real-world navigation studies in rodents. Therefore, applying the BOSC method allowed for direct comparisons of our findings with previously published results.

For each participant and within each trial, data were separated into low- and high-speed movements using a median split on speed in that trial to obtain an equal amount of data within each condition (see the STAR Methods). By utilizing the BOSC method [28, 29], episodes with significant oscillations between 3 and 30 Hz (p-episodes, percentage trial time in oscillatory episodes [29]; occurring for at least 3 cycles and above 95% chance level; Figure 4A) were calculated in frequency windows of 0.25 Hz (see the STAR Methods). We found that, in all 4 participants, there was a significant increase in theta oscillations during fast movements compared to slow movements (Figure 4B). This increase in the prevalence of theta, as quantified by p-episodes, was observed between 7 and 9.25 Hz ($N_{trials \times channels} = 84$; $p < 0.05$, clustered-based permutation test [32]; see the STAR Methods) for the sighted participants and between 6.5 and 8.75 Hz in the congenitally blind

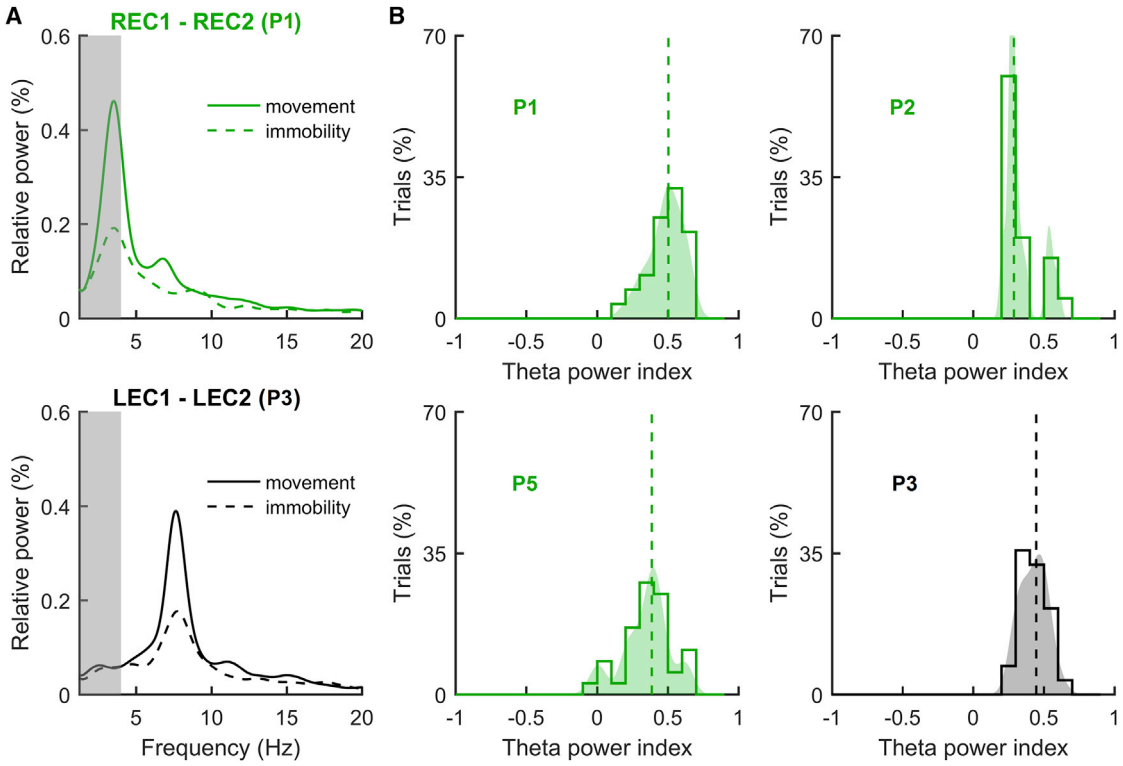

Figure 3. Theta Power during Movement versus Periods of Immobility

(A) Example (normalized) power spectra from a sighted participant (P1, top, green) and the congenitally blind participant (P3, bottom, black) displaying more theta power during movement (solid lines) compared to immobility (dashed lines). The power spectrum for each trial was normalized by the average power in that trial, during movement and immobility, over the frequency range 3–12 Hz. Values below 4 Hz (lower range of the analog bandpass filter) are marked with shaded gray areas. Channel names are labeled clinically, and for a detailed description, see Table S3. The recordings were bipolar using adjacent electrodes 1-2 and 3-4 (e.g., REC1-REC2 is one iEEG channel). The two adjacent electrodes in iEEG channel REC1-REC2 in participant P1 were located in the right entorhinal cortex (REC1) and right perirhinal cortex (REC2). The two adjacent electrodes in iEEG channel LEC1-LEC2 in participant P3 were located in the left entorhinal cortex (LEC1) and left perirhinal cortex (LEC2).

(B) Theta power index was significantly positive for all participants as shown above, thus indicating higher theta power during movement (sighted participants, green; P1: 0.50, [0.43, 0.57], $p = 3.79 \times 10^{-16}$; P2: 0.29, [0.27, 0.36], $p = 8.86 \times 10^{-5}$; P5: 0.39, [0.24, 0.43], $p = 2.36 \times 10^{-7}$; congenitally blind participant, black; P3: 0.45, [0.35, 0.50], $p = 3.79 \times 10^{-6}$; Wilcoxon signed-rank test was used because not all of the distributions passed the Lilliefors test of normality). Shaded area corresponds to kernel smoothing function estimate of the distribution and the dashed line indicates the median value.

See also Figure S2 and Table S3.

participant ($N_{trials \times channels} = 28$; $p < 0.05$, clustered-based permutation test; note that these ranges were qualitatively similar using Wilcoxon rank-sum test). Interestingly, these theta episodes were transient and present ~10% of the time for the sighted group, while this percentage was ~30% in the congenitally blind participant (Figure 4B). Hence, we analyzed the data from the congenitally blind participant separately from the data from sighted participants, whose results were qualitatively similar to each other (Figure S3A). Moreover, we observed significant differences in p-episodes in higher frequencies (17.25–18.25 Hz in sighted participants and 14.5–16.75 Hz in the congenitally blind participant; clustered-based permutation test) (Figure 4B). This might suggest the presence of theta harmonics in our data, which have been reported to increase with movement speed in rats [33].

The differences in the prevalence of theta oscillations between the blind and sighted participants called for an assessment of sighted participants walking with their eyes closed. To address this, two of our participants (P1 and P5) performed the task while they were blindfolded and had their eyes closed. Although the overall speed was generally lower (median, [25^{th}, 75^{th}] = 0.28, [0.02, 0.60] m/s), we found no qualitative differences in theta properties between the conditions with closed or open eyes (Figure S3B). This suggests that the congenitally blind participant may have developed a different strategy for navigating an environment that may not be readily available to sighted participants. We then asked whether there was a strategy that would result in higher prevalence of theta oscillations. To address this, we asked a participant (P5) to walk back and forth on the same path while head-scanning left and right or looking at a fixed target on the wall. Here, we found that theta oscillations were more present during head-scanning behavior, quantified by larger angular speed of the participant's head (Figure 5; p-episode = 21.73% ± 4.47% at peak frequency of 7.75 Hz versus p-episode = 10.09% ± 3.85% during walking while looking at a fixed target).

It is worth noting that there is an analog filter on the RNS System, equivalent to a first-order Butterworth with 3 dB

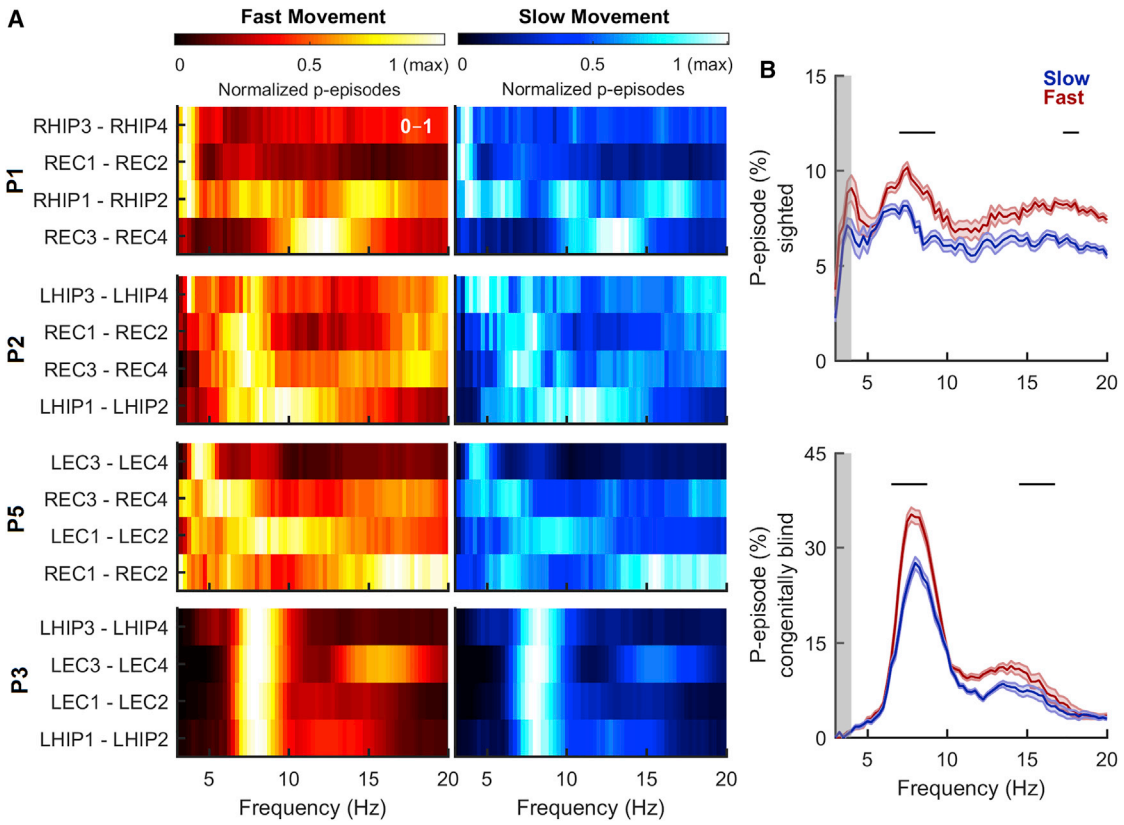

Figure 4. Significant Increase in the Prevalence of High-Frequency Theta Oscillations during Fast Compared to Slow Movement

(A) Color map shows percentage of time with significant oscillations (p-episode) in the frequency range indicated on the x axis averaged across trials for each clinically labeled channel in the left entorhinal cortex (LEC) and right entorhinal cortex (REC) and left hippocampus (LHIP) and right hippocampus (RHIP) from all participants (electrode 1, most distal; electrode 4, most proximal). The electrodes were implanted orthogonally to the surface of the brain; thus, distal and proximal correspond to deeper and shallower contacts, respectively). Channel names are labeled clinically; for a detailed description of the localizations, see Table S3. Data are normalized by the maximum value for each channel, within each condition, for visibility purposes (range: 0–1). Brighter colors indicate larger values as demonstrated by the colorbars. Throughout this figure, red shades and blue shades correspond to fast and slow movements, respectively. Also, note that, for each participant, channels are sorted based on the frequency with maximum prevalence during fast movements, i.e., the frequency with maximum p-episodes in each channel increases from top to bottom rows. Left: shown are the normalized p-episodes during fast movement (N_{trials} for participants P1, P2, P5, and P3 (congenitally blind) were 7, 5, 9, and 7, respectively). Right: shown are the same as at left but during movement at slow speeds.

(B) Percentage of time with significant oscillations (across all trials and channels; shown are mean ± SEM) during fast movements (red) versus slow movements (blue) in 3 sighted participants (top, $N_{trials \times channels} = 84$) and 1 congenitally blind participant (bottom, $N_{trials \times channels} = 28$). Black horizontal lines indicate regions with significant difference in p-episodes between fast and slow movement conditions ($p < 0.05$, clustered-based permutation test). Values below 4 Hz (lower range of the analog bandpass filter) are marked with shaded gray areas.

See also Figures S3–S5 and Table S3.

attenuation at the cutoff frequencies (4–90 Hz). Thus, it was necessary to test and validate our results to ensure that they were not an artifact of the filter. First, we used broadband data (0.1–8,000 Hz) recorded from an independent group of participants (n = 2), from a previous study by Suthana et al. [34], who were acutely implanted with depth electrodes for seizure monitoring during inpatient hospitalization (hereinafter referred to as depth subjects). Here, we confirmed that the BOSC method returned highly similar results, both in calculating power spectra and oscillation detection patterns, in the presence or absence of a mathematically implemented filter analogous to the one on the RNS System (Figures S4A and S4B; see the STAR Methods). Second, to further ensure that our results were not skewed by the analog filter on the RNS Ssystem, we collected broadband data (0.1–8,000 Hz) recorded from a single depth subject during movement. The participant was asked to walk slowly around his hospital room as we tracked his motion using Google's Project Tango tablet (see the STAR Methods), which allowed us to perform the same analyses we used in participants with the RNS System (Figure S4C). We used data from an electrode contact (macro-electrode; see the STAR Methods) that fell within the MTL region (CA1) for further analysis. Due to the small variability in the walking speed, caused by the participant having to navigate in limited space around hospital equipment while tethered, we compared p-episodes using the BOSC method during periods of movement versus immobility. Here, too, our results showed a qualitatively similar percentage of time with significant theta oscillation during movement, and they

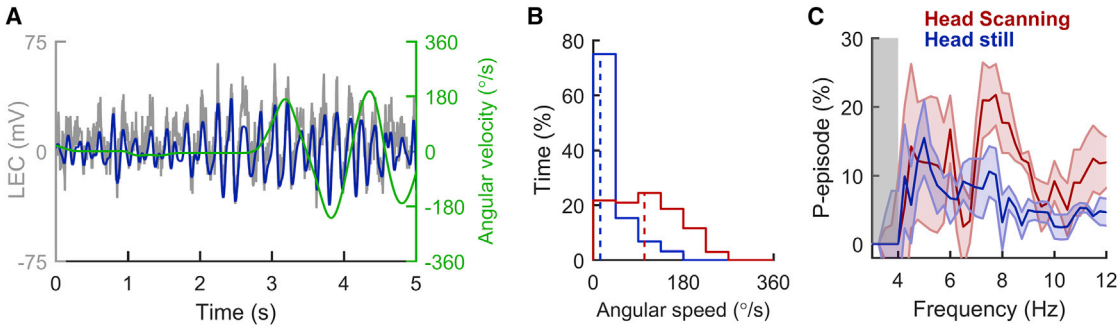

Figure 5. Theta Oscillations Are More Prevalent during Head-Scanning Behavior

(A) Example raw iEEG trace (gray) from a participant (P5) overlaid with filtered (3–12 Hz) theta oscillations (blue) while he walked down the same path with and without head-scanning left and right. Green trace demonstrates the angular velocity of the head.

(B) The participant was able to perform the task, and periods with head-scanning behavior (red) manifested higher head angular speed (dashed line denotes the median value).

(C) Head-scanning behavior resulted in higher presence of theta oscillations (red curve, p-episode = 21.73% ± 4.47% at peak frequency of 7.75 Hz) compared to periods when the participant walked looking at a fixed target (blue curve, p-episode = 10.09% ± 3.85% at 7.75 Hz). Shown are the mean ± SEM values. Values below 4 Hz (lower range of the analog bandpass filter) are marked with shaded gray areas.

demonstrated that higher frequency theta is more prevalent during movement versus immobility (Figure S4D), thus indicating that our oscillation detection method is robust.

Duration of Oscillatory Bouts

We next asked whether the increase in the prevalence of theta during fast versus slow movements was due to longer theta bouts or higher rates of occurrence. To address this, we computed the duration of oscillatory bouts by varying the threshold for the number of cycles required for significance (Figure 6A). We detected significant oscillatory episodes with at least one cycle, converted the total number of detected cycles in each bout to durations, and computed the average durations of these epochs in each frequency bin. Comparisons of the durations of theta bouts in fast and slow movements showed no significant difference in bout durations between the two conditions ($p > 0.05$ at any frequency, cluster-based permutation test) (Figure 6B). This suggests that more prevalent theta during fast movement potentially arises as a result of short theta bouts of similar lengths occurring more frequently during fast movements. We also observed that the average duration of theta bouts was higher in the congenitally blind participant (~570 ms) compared to sighted participants (440 ms) at the peak frequency (Figure 6B). It is worth mentioning that, by comparing our results with those published by Watrous et al. [31] using the same method (see Figure 2D in [31]), it is evident that our results from the blind participant are more similar to those observed in moving rodents. Moreover, our findings in sighted participants lie between rodent real-world navigation and human virtual navigation, further supporting the hypothesis that the observed theta oscillations in the current study are indeed movement related.

To test whether the movement speed (i.e., fast versus slow movement) can be decoded from the pattern of oscillations, we used a neural network machine-learning model, a commonly used method for classification that is generally more flexible compared to other methods, such as logistic regression [35] (see the STAR Methods). Here, power spectra—computed using wavelet analysis present in the BOSC method toolbox (Figure S5A; see the STAR Methods)—were used as the input to our model in order to predict movement speed (Figure S5B). Data were divided into independent sets for training, cross-validation (to reduce overfitting), and testing. Receiver operating characteristic (ROC) plots and the area under these curves (AUC)—common measures of model performance in classification [36]—showed that the performance of our model was significantly better than chance in classifying fast from slow movement speeds (Figure S5C).

DISCUSSION

We present a novel, innovative methodology for combining motion capture technology and continuous iEEG recordings, enabling access to the MTL in freely moving humans. To our knowledge, this study demonstrates the first quantification of theta oscillations during untethered ambulatory movement in humans. Our results show that high-frequency (~8 Hz) theta oscillations occur during movement and exhibit a higher power compared to periods of immobility. In addition, theta occurs in short bouts (~400 ms) that are present more frequently during fast versus slow movement speeds and, thus, significantly differentiate the two.

Previous investigations of theta oscillations in primates have resulted in conflicting evidence regarding the presence and functionality of the theta rhythm compared to those in rodents [19, 31, 37, 38]. These dissimilarities are thought to be, in part, attributed to the differences in the primary source of sensory information in these species—visual inputs in primates versus olfactory and somatosensory inputs in rodents. Nonetheless, the lack of feasibility in recording iEEG in freely moving primates (in contrast to rodents) has not previously allowed for unequivocal evaluation of theta oscillatory properties under similar conditions in these species. Our findings demonstrate that, in humans, short, intermittent theta bouts occur and are indeed movement-related, but they are not as continuous as those found in rodents. Further, these bouts occur at a higher rate

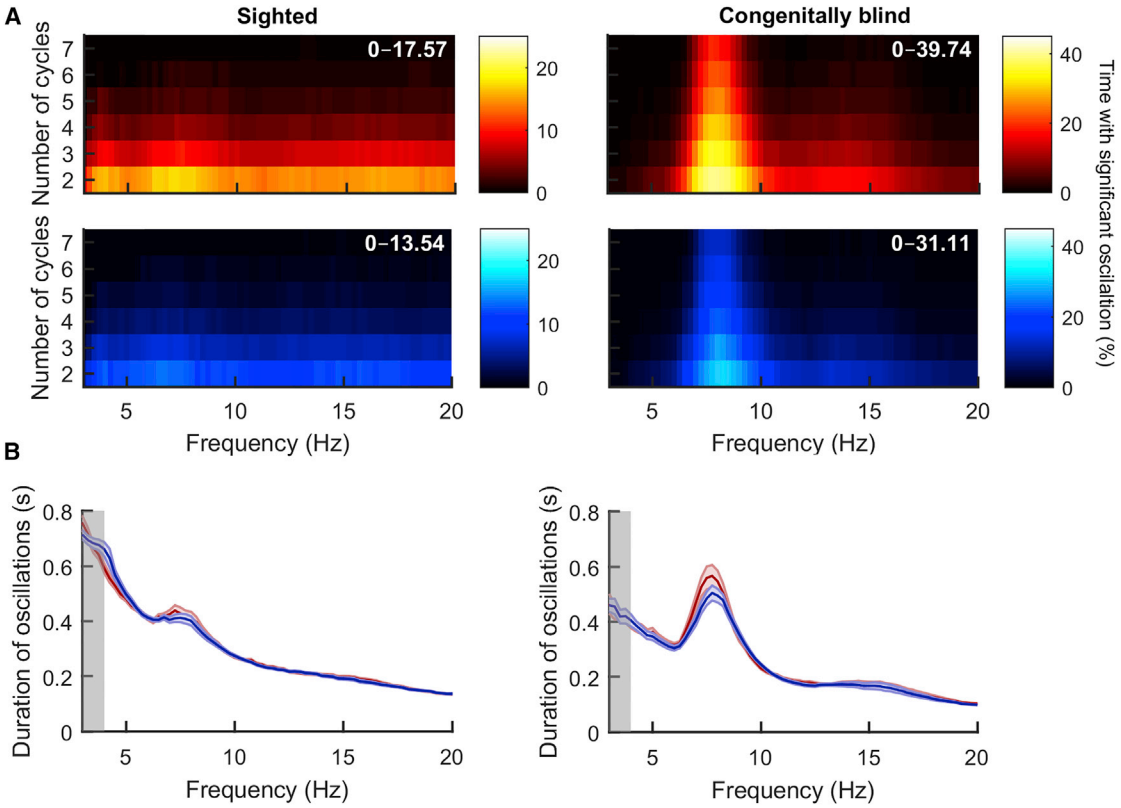

Figure 6. Duration of Theta Bouts Is Similar during Fast and Slow Movements

(A) Color maps indicate percentage of time with significant oscillations (p-episodes) in each frequency (averaged across trials, channels, and participants), assuming varying number of minimum cycles for detection (y axis). Red and blue color schemes correspond to fast and slow movements, respectively, here and throughout the figure. Number at the top right corner indicates range.

(B) Duration of significant oscillations at each frequency is shown as mean ± SEM across all trials and channels. There was no significant difference between the duration of the bouts between fast (red) and slow (blue) movements. However, note that, in the congenitally blind participant (right), the duration of theta bouts (0.57 s at peak frequency of 7.75 Hz) was longer than those in the sighted participants (left, 0.44 s at peak frequency of 7.25 Hz). Values below 4 Hz (lower range of the analog bandpass filter) are marked with shaded gray areas.

during fast movements. One possible explanation for this effect is that saccadic eye movements are the dominant source of sensory input as a means for exploration in primates [16, 19, 38]. Thus, if saccadic eye movements occur at a higher rate during faster locomotion, this could potentially lead to more frequent theta bouts. Whether theta bouts are elicited and phase-reset by saccades warrants further investigation.

Curiously, in our present results, significant theta oscillations occurred more often and more continuously in a single participant who is congenitally blind. This participant used a Hoover cane to traverse the environment, thereby possibly using somatosensory and path-integration inputs to a greater extent compared to other normally sighted participants. This may support the idea that the modality of sensory processing may be a critical factor relating theta oscillations to movement. Alternatively, it is argued that theta oscillations facilitate multisensory integration during active explorations and, thus, the differences between the blind participant and the sighted participants could have arisen as a result of how often exploration is required for navigation [16, 38]. Given that somatosensory and path-integration cues—used by the blind participant and even rats—are more local compared to the distal visual cues (used by the sighted participants), they might be engaged more frequently during navigation. This might elucidate why theta in sighted humans is less continuous than theta in the blind participant and in rats, and also it might explain why theta oscillations are present more often during fast movements compared to slow movements, and during head-scanning behavior.

While, on average, the prevalence of theta oscillations was higher during fast versus slow movement, we observed differences in oscillation frequencies across regions and within individuals (Figure 4A). Thus, it is possible that there are subtle differences in oscillatory properties across MTL regions, which are not captured within our study. For example, in rodents, it has been shown that the frequency of theta oscillations decreases—albeit slightly—along the septotemporal axis of the hippocampus, and a similar decrease has been found in the dorsoventral axis of the entorhinal cortex [39–41]. Another recent study demonstrated that nonlinear dynamics of theta oscillations in rodents vary with movement speed and are modulated by hippocampal regions [33]. Lastly, theta oscillations are diminished in power and spatial selectivity is reduced in the ventral compared to dorsal hippocampus [40]. In humans, the dorsoventral distinction is thought to map onto

the posterior-anterior hippocampal axis [42]. Therefore, future larger sample studies will be necessary to characterize movement-related theta changes across MTL regions and the implications of these differences in the coordinating role of theta oscillations.

Recently, it has been argued that the human analog of rodent theta oscillations exists in the lower (<4 Hz) frequency range [37]. However, to our knowledge, the investigation of theta oscillations within the human MTL during real-world ambulatory movement has been limited due to the restrictions of wired intracranial recording electrode technology and the electrical noise introduced in the recordings as a result of physical movement. Using wireless, chronically implanted electrodes, our results suggest there does, in fact, exist a higher frequency (~8 Hz) theta oscillation in the human MTL associated with physical movement—a finding that was replicated in an independent study [22]. Furthermore, lower frequency theta (~4 Hz) in humans has been observed in stationary virtual navigation and memory tasks [43–46]. However, due to the analog filter on the RNS System, the current study cannot address the differences between the two types of theta oscillations, and future studies are needed to determine how low- and high-frequency theta dynamics interact during ambulatory movement compared to those in stationary behavioral tasks. While the high-frequency theta presented in the current study varies significantly between different speeds of movement, its exact behavioral correlates remain to be examined. It must be borne in mind that the study participants were epilepsy patients with altered cognitive functions. Although the task employed in this study was not related to memory and, consequently, all participants successfully performed the task, the relationship between theta oscillations and memory performance warrants further investigation in future experiments with memory demands.

Overall, the current study provides important insight into human MTL theta oscillations during ambulatory behavior, and, by elucidating similarities as well as differences in theta dynamics, it can bridge findings across species. We present a novel paradigm for the leveraging of FDA-approved technology combined with motion tracking that allows for future investigation of neural oscillatory dynamics during real-world behaviors in humans.

STAR★METHODS

Detailed methods are provided in the online version of this paper and include the following:

- KEY RESOURCE TABLE
- CONTACT FOR REAGENT AND RESOURCE SHARING
- EXPERIMENTAL MODEL AND SUBJECT DETAILS
  - Participants implanted with the RNS System
  - Depth subjects
- METHOD DETAILS
  - Data acquisition
  - Electromagnet
  - Motion tracking
  - Synchronization of iEEG and motion capture data
  - Electrode Localization
  - Behavioral task
- QUANTIFICATION AND STATISTICAL ANALYSIS
  - Elimination of epileptic activity from iEEG
  - Theta power index
  - Generalized estimating equations (GEE)
  - Detection of significant oscillations
  - Control analysis for oscillation detection
  - Extraction of theta from iEEG
  - Statistics
  - Classification of movement speed using machine learning
- DATA AND SOFTWARE AVAILABILITY

SUPPLEMENTAL INFORMATION

Supplemental Information includes six figures, three tables, and three movies and can be found with this article online at https://doi.org/10.1016/j.cub.2017.10.062.

AUTHOR CONTRIBUTIONS

Z.M.A., I.F., and N.S. conceived the research. Z.M.A. and N.S. designed the research. Z.M.A., P.S., M.E.T., S.M.S., and N.S. performed analyses. Z.M.A., P.S., E.A.M., and N.S. collected data and performed research. Z.M.A., T.A.F., N.R.H., T.K.T., and N.S. designed and implemented technical tools. D.E. and J.S. provided clinical procedures. I.F. performed all implantation of the RNS and depth electrodes. Z.M.A., E.A.M., I.F., and N.S. wrote the paper. All the authors commented on the manuscript.

ACKNOWLEDGMENTS

This work was supported by UCLA startup funds (principal investigator: N.S.) and grants from the DARPA Restoring Active Memory program (N66001-14-2-4029; principal investigator: I.F.), the National Institute of Neurological Disorders and Stroke (NS058280 to Z.M.A and E.A.M., and NS084017 to I.F.), and the A.P. Giannini Foundation to E.A.M. We thank Eric Behnke for technical assistance, Brooke Salaz for general assistance, Fabien Scalzo for useful discussions, and the participants for volunteering for this study. T.K.T. and N.R.H. are employees of NeuroPace, Inc.

Received: July 10, 2017
Revised: September 21, 2017
Accepted: October 25, 2017
Published: November 30, 2017

REFERENCES

1. Squire, L.R. (1992). Memory and the hippocampus: a synthesis from findings with rats, monkeys, and humans. Psychol. Rev. *99*, 195–231.
2. Squire, L.R., Stark, C.E.L., and Clark, R.E. (2004). The medial temporal lobe. Annu. Rev. Neurosci. *27*, 279–306.
3. Buzsáki, G., and Moser, E.I. (2013). Memory, navigation and theta rhythm in the hippocampal-entorhinal system. Nat. Neurosci. *16*, 130–138.
4. Jutras, M.J., and Buffalo, E.A. (2014). Oscillatory correlates of memory in non-human primates. Neuroimage *85*, 694–701.
5. Colgin, L.L. (2016). Rhythms of the hippocampal network. Nat. Rev. Neurosci. *17*, 239–249.
6. Buzsaki, G. (2006). Rhythms of the Brain (Oxford University Press).
7. Vanderwolf, C.H. (1969). Hippocampal electrical activity and voluntary movement in the rat. Electroencephalogr. Clin. Neurophysiol. *26*, 407–418.
8. Robinson, T.E., Kramis, R.C., and Vanderwolf, C.H. (1977). Two types of cerebral activation during active sleep: relations to behavior. Brain Res. *124*, 544–549.

9. Berry, S.D., and Thompson, R.F. (1978). Prediction of learning rate from the hippocampal electroencephalogram. Science *200*, 1298–1300.
10. Klimesch, W., Doppelmayr, M., Russegger, H., and Pachinger, T. (1996). Theta band power in the human scalp EEG and the encoding of new information. Neuroreport *7*, 1235–1240.
11. Seager, M.A., Johnson, L.D., Chabot, E.S., Asaka, Y., and Berry, S.D. (2002). Oscillatory brain states and learning: Impact of hippocampal theta-contingent training. Proc. Natl. Acad. Sci. USA *99*, 1616–1620.
12. Winson, J. (1978). Loss of hippocampal theta rhythm results in spatial memory deficit in the rat. Science *201*, 160–163.
13. Canolty, R.T., and Knight, R.T. (2010). The functional role of cross-frequency coupling. Trends Cogn. Sci. *14*, 506–515.
14. Hasselmo, M.E. (2005). What is the function of hippocampal theta rhythm?–Linking behavioral data to phasic properties of field potential and unit recording data. Hippocampus *15*, 936–949.
15. Bland, B.H., Sainsbury, R.S., and Creery, B.L. (1979). Anatomical correlates of rhythmical slow wave activity (theta) in the hippocampal formation of the cat. Brain Res. *161*, 199–209.
16. Ulanovsky, N., and Moss, C.F. (2007). Hippocampal cellular and network activity in freely moving echolocating bats. Nat. Neurosci. *10*, 224–233.
17. Yartsev, M.M., and Ulanovsky, N. (2013). Representation of three-dimensional space in the hippocampus of flying bats. Science *340*, 367–372.
18. Stewart, M., and Fox, S.E. (1991). Hippocampal theta activity in monkeys. Brain Res. *538*, 59–63.
19. Jutras, M.J., Fries, P., and Buffalo, E.A. (2013). Oscillatory activity in the monkey hippocampus during visual exploration and memory formation. Proc. Natl. Acad. Sci. USA *110*, 13144–13149.
20. Lega, B.C., Jacobs, J., and Kahana, M. (2012). Human hippocampal theta oscillations and the formation of episodic memories. Hippocampus *22*, 748–761.
21. Ekstrom, A.D., Caplan, J.B., Ho, E., Shattuck, K., Fried, I., and Kahana, M.J. (2005). Human hippocampal theta activity during virtual navigation. Hippocampus *15*, 881–889.
22. Bohbot, V.D., Copara, M.S., Gotman, J., and Ekstrom, A.D. (2017). Low-frequency theta oscillations in the human hippocampus during real-world and virtual navigation. Nat. Commun. *8*, 14415.
23. Ravassard, P., Kees, A., Willers, B., Ho, D., Aharoni, D.A., Cushman, J., Aghajan, Z.M., and Mehta, M.R. (2013). Multisensory control of hippocampal spatiotemporal selectivity. Science *340*, 1342–1346.
24. Aghajan, Z.M., Acharya, L., Moore, J.J., Cushman, J.D., Vuong, C., and Mehta, M.R. (2015). Impaired spatial selectivity and intact phase precession in two-dimensional virtual reality. Nat. Neurosci. *18*, 121–128.
25. Gelinas, J.N., Khodagholy, D., Thesen, T., Devinsky, O., and Buzsáki, G. (2016). Interictal epileptiform discharges induce hippocampal-cortical coupling in temporal lobe epilepsy. Nat. Med. *22*, 641–648.
26. Hardin, J.W. (2005). Generalized estimating equations (GEE). In Encyclopedia of Statistics in Behavioral Science, B.S. Everitt, and D. Howell, eds. (John Wiley & Sons).
27. Hubbard, A.E., Ahern, J., Fleischer, N.L., Van der Laan, M., Lippman, S.A., Jewell, N., Bruckner, T., and Satariano, W.A. (2010). To GEE or not to GEE: comparing population average and mixed models for estimating the associations between neighborhood risk factors and health. Epidemiology *21*, 467–474.
28. Hughes, A.M., Whitten, T.A., Caplan, J.B., and Dickson, C.T. (2012). BOSC: a better oscillation detection method, extracts both sustained and transient rhythms from rat hippocampal recordings. Hippocampus *22*, 1417–1428.
29. Caplan, J.B., Madsen, J.R., Raghavachari, S., and Kahana, M.J. (2001). Distinct patterns of brain oscillations underlie two basic parameters of human maze learning. J. Neurophysiol. *86*, 368–380.
30. Whitten, T.A., Hughes, A.M., Dickson, C.T., and Caplan, J.B. (2011). A better oscillation detection method robustly extracts EEG rhythms across brain state changes: the human alpha rhythm as a test case. Neuroimage *54*, 860–874.
31. Watrous, A.J., Lee, D.J., Izadi, A., Gurkoff, G.G., Shahlaie, K., and Ekstrom, A.D. (2013). A comparative study of human and rat hippocampal low-frequency oscillations during spatial navigation. Hippocampus *23*, 656–661.
32. Maris, E., and Oostenveld, R. (2007). Nonparametric statistical testing of EEG- and MEG-data. J. Neurosci. Methods *164*, 177–190.
33. Sheremet, A., Burke, S.N., and Maurer, A.P. (2016). Movement Enhances the Nonlinearity of Hippocampal Theta. J. Neurosci. *36*, 4218–4230.
34. Suthana, N.A., Parikshak, N.N., Ekstrom, A.D., Ison, M.J., Knowlton, B.J., Bookheimer, S.Y., and Fried, I. (2015). Specific responses of human hippocampal neurons are associated with better memory. Proc. Natl. Acad. Sci. USA *112*, 10503–10508.
35. Dreiseitl, S., and Ohno-Machado, L. (2002). Logistic regression and artificial neural network classification models: a methodology review. J. Biomed. Inform. *35*, 352–359.
36. Huang, J., and Ling, C.X. (2005). Using AUC and accuracy in evaluating learning algorithms. IEEE Trans. Knowl. Data Eng. *17*, 299–310.
37. Jacobs, J. (2013). Hippocampal theta oscillations are slower in humans than in rodents: implications for models of spatial navigation and memory. Philos. Trans. R. Soc. Lond. B Biol. Sci. *369*, 20130304.
38. Geva-Sagiv, M., Las, L., Yovel, Y., and Ulanovsky, N. (2015). Spatial cognition in bats and rats: from sensory acquisition to multiscale maps and navigation. Nat. Rev. Neurosci. *16*, 94–108.
39. Hasselmo, M.E., Giocomo, L.M., and Zilli, E.A. (2007). Grid cell firing may arise from interference of theta frequency membrane potential oscillations in single neurons. Hippocampus *17*, 1252–1271.
40. Royer, S., Sirota, A., Patel, J., and Buzsáki, G. (2010). Distinct representations and theta dynamics in dorsal and ventral hippocampus. J. Neurosci. *30*, 1777–1787.
41. Patel, J., Fujisawa, S., Berényi, A., Royer, S., and Buzsáki, G. (2012). Traveling theta waves along the entire septotemporal axis of the hippocampus. Neuron *75*, 410–417.
42. Strange, B.A., Witter, M.P., Lein, E.S., and Moser, E.I. (2014). Functional organization of the hippocampal longitudinal axis. Nat. Rev. Neurosci. *15*, 655–669.
43. Kahana, M.J., Seelig, D., and Madsen, J.R. (2001). Theta returns. Curr. Opin. Neurobiol. *11*, 739–744.
44. Jacobs, J., and Kahana, M.J. (2010). Direct brain recordings fuel advances in cognitive electrophysiology. Trends Cogn. Sci. *14*, 162–171.
45. Buzsáki, G. (2005). Theta rhythm of navigation: link between path integration and landmark navigation, episodic and semantic memory. Hippocampus *15*, 827–840.
46. Rutishauser, U., Ross, I.B., Mamelak, A.N., and Schuman, E.M. (2010). Human memory strength is predicted by theta-frequency phase-locking of single neurons. Nature *464*, 903–907.
47. Jenkinson, M., and Smith, S. (2001). A global optimisation method for robust affine registration of brain images. Med. Image Anal. *5*, 143–156.
48. Gumprecht, H.K., Widenka, D.C., and Lumenta, C.B. (1999). BrainLab VectorVision Neuronavigation System: technology and clinical experiences in 131 cases. Neurosurgery *44*, 97–104.
49. Yushkevich, P.A., Wang, H., Pluta, J., Das, S.R., Craige, C., Avants, B.B., Weiner, M.W., and Mueller, S. (2010). Nearly automatic segmentation of hippocampal subfields in in vivo focal T2-weighted MRI. Neuroimage *53*, 1208–1224.

STAR★METHODS

KEY RESOURCE TABLE

REAGENT or RESOURCE	SOURCE	IDENTIFIER
Software and Algorithms		
IBM SPSS Statistics 24	IBM Analytics	RRID: SCR_002865; https://www.ibm.com/products/spss-statistics
MATLAB R2016A	The MathWorks	RRID: SCR_001622; http://www.mathworks.com/products/matlab/
BOSC Toolbox	[30]	https://ars.els-cdn.com/content/image/1-s2.0-S1053811910011614-mmc1.zip
Custom MATLAB and SPSS scripts for statistical tests	This paper	Request from Lead Contact

CONTACT FOR REAGENT AND RESOURCE SHARING

Further information and requests should be directed to and will be fulfilled by the Lead Contact, Nanthia Suthana (nsuthana@mednet.ucla.edu).

EXPERIMENTAL MODEL AND SUBJECT DETAILS

Participants implanted with the RNS System

Participants (Table S1) were 4 patients (three sighted and one congenitally blind) with pharmacoresistant epilepsy who had been previously implanted with the FDA approved NeuroPace RNS System for treatment of epilepsy. The congenitally blind participant exhibited lifelong visual impairment with marginal light perception due to retinopathy of prematurity. Electrode placements were determined solely based on clinical treatment criteria. All participants volunteered for the study by providing informed consent according to a protocol approved by the UCLA Medical Institutional Review Board (IRB). Neuropsychological scores for each individual were determined using methods previously described [34] (Table S2).

Depth subjects

Participants were patients with pharmacoresistant epilepsy who were implanted with depth-electrodes for seizure monitoring. Electrophysiological data were recorded at 40 KHz using ATLAS Data Acquisition system (Neuralynx, Bozeman, MT). A subset of the data was recorded and used in a previous study [34]. In addition, one depth subject was asked to walk back and forth in the hospital room (tethered) while holding Google's Project Tango tablet, which was equipped with motion tracking (https://get.google.com/tango/). The Paraview Tango Recorder application (https://blog.kitware.com/paraview-and-project-tango-loading-data/) was utilized to track their position. Data from a macro-electrode contact (1.5 mm diameter and surface area = 5.9 mm^2) located within the MTL region (CA1) (see Electrode localization methods) were used for further analysis.

METHOD DETAILS

Data acquisition

The FDA approved NeuroPace RNS System (Figure 1A) is designed to be programmed to detect abnormal electrical activity in the brain and respond in a closed loop manner by delivering imperceptible levels of electrical stimulation intended to normalize brain activity before an individual experiences seizures. For the present study, a neurologist was present to configure stimulation to OFF and ON before and after the study and monitor for seizure activity. Each of the 4 participants in the study had two implanted depth electrode leads 1.27 mm in diameter each with 4 platinum-iridium electrode contacts, each with a surface area of 7.9 mm^2, 1.5 mm long with an electrode spacing of either 3.5 or 10 mm (Table S3). During the study, the RNS Neurostimulator continuously monitored iEEG activity on four bipolar channels at 250 Hz with an analog filter equivalent to a 1^{st} order Butterworth with 3 dB attenuation at the cutoff frequencies (4–90 Hz). The neurostimulator communicates wirelessly with a Programmer and Remote Monitor using secure protocols. The Programmer is used to (1) retrieve data, including stored iEEG data, from the neurostimulator, (2) configure detection and stimulation, and (3) monitor iEEG activity and test stimulation settings in real-time. A programmable electromagnet was used to trigger iEEG storage in the RNS Neurostimulator.

Electromagnet

A programmable electromagnet was designed to be placed on the participant's head over the RNS Neurostimulator and trigger iEEG recordings by generating magnetic pulses. The magnetic pulses could be triggered either manually or automatically with programmable intervals of 30, 60, 90, 150, 180 and 240 s. Power was provided by rechargeable NICAD batteries. The electromagnet had a visible LED as well as an infrared LED, which were used both as visible indicators and event markers for synchronization of iEEG recordings with recorded video. The device accepts three commands: a hard reset command, which allows for either alteration of the timing or entering into the test mode; a clear command which is a soft reset in that any command other than reset is halted and all timing counters are cleared; and a start or stop command which starts the timing for the marker function.

Motion tracking

Motion tracking was done using the Optitrack system (Natural Point, Inc.; http://optitrack.com/) with 8 ceiling mounted infrared high-resolution cameras that allow for sub-millimeter motion tracking. Removable reflective markers were used in conjunction with specialized software, Motive and Camera SDK, which allowed for kinematic labeling. For the head, a rigid body object was constructed, from the reflective markers, for which the center of mass (i.e., position) was tracked in addition to a quaternion describing rotational information that was translated to Euler angles to obtain yaw, pitch, and roll with respect to the experimental room. This information was then used to obtain participants' movement trajectory and speed (Figures 1B–1D). Further, another set of 4 ceiling mounted high-resolution Optitrack cameras were dedicated to record videos in the visible spectrum, which were then used for synchronization purposes (see below).

Synchronization of iEEG and motion capture data

When the electromagnet was activated, it triggered the storage of iEEG data by the RNS System in preconfigured short durations (60 s), generated a "magnet marker" event in the iEEG data, as well as turned on a visible LED light, which was captured by the video cameras. The "magnet marker" events in the iEEG data were then aligned with the onset of the visible LED light events in our motion tracking system. This allowed us to synchronize the two data streams and combine the stored pieces of iEEG data into a long continuous recording.

Electrode Localization

Electrode localization was done using methods similar to those reported by Suthana et al. [34]. A high-resolution post-operative CT image was co-registered to a pre-operative whole brain and high-resolution MRI for each participant (Figure 2B; Figure S6). We used the FSL FLIRT (FMRIB's Linear Registration Tool [47]) together with BrainLab stereotactic and localization software [48]. MTL regions (entorhinal, perirhinal, parahippocampal, hippocampal subfields CA23DG [CA2, 3, dentate gyrus], CA1, and subiculum) are anatomically determined by boundaries that are demarcated based on atlases correlating MRI visible landmarks with underlying cellular histology. To avoid human bias and perform hippocampal segmentation programmatically we used ASHS software [49].

Behavioral task

Participants performed a task in which they were directed to walk at slow or fast speeds following linear and circular paths in a 400 square foot room based on an auditory command. Each trial consisted of four different conditions: walking in straight lines or circles at slow or fast speeds, and the order in which these conditions were presented was randomized. This strategy yielded a relatively large range of movement speeds (Figure 1D). Furthermore, for each participant, the speed profile was similar across different trials (data not shown).

QUANTIFICATION AND STATISTICAL ANALYSIS

All analyses were performed offline using custom code in MATLAB and SPSS.

Elimination of epileptic activity from iEEG

Data from putative epileptic epochs were discarded according to a method similar to procedures described recently [25] using functions found in MATLAB Signal Processing Toolbox. In brief, epileptic discharges were identified when either of the following conditions were satisfied: a) the envelope of the unfiltered signal was 5 s.d. above the baseline; b) the envelope of the filtered signal (band-pass filtered in the 25–80 Hz range followed by signal rectification) was 6 s.d. above the baseline (Figure S1). We excluded ~3% of the data from further analysis because of the presence of epileptic activity and this percentage was not significantly different between slow and fast movements ($p = 0.6$, Wilcoxon rank-sum test; Figure S1B). All of the iEEG traces used for analysis were also visually inspected for epileptic activity, before and after the automatic removal procedure.

Theta power index

For each trial, the theta power index was computed by subtracting the total power between 3–12 Hz, henceforth referred to as theta power, during immobility from theta power during movement and normalizing the resulting value by the sum:

$$\theta \text{ power index} = \frac{\theta_{movement} - \theta_{immobility}}{\theta_{movement} + \theta_{immobility}}.$$

This measure varies between −1 and 1 with positive values indicating more theta power during movement.

Generalized estimating equations (GEE)

We used GEE, a class of regression marginal models, to examine the relationship between relative theta power and movement while accounting for potential clustering between the data points due to the within-subject repeated-measure design. Here, relative theta power was modeled using SPSS software (IBM Corporation, USA) with a movement condition (movement versus immobility) as a predictor. We implemented the model with participant identity as a within-subject variable, exchangeable correlation matrix with robust covariance estimate, and using linear scale response (identity link function). Model statistics are reported as the estimated means and 95% Wald confidence intervals.

Detection of significant oscillations

BOSC algorithm was used [28–30], and episodes with significant oscillations (using 6th order wavelets and for bouts occurring for at least 3 cycles and above 95% chance level) were detected. Additionally, to examine the duration of theta bouts, the lower bound on the number of cycles for detection was allowed to vary.

Control analysis for oscillation detection

To evaluate the effect of the analog bandpass filter (1st order Butterworth 4–90 Hz, 3 dB attenuation at cutoff frequencies) on the RNS System on our results, we mathematically implemented this filter on data collected from a previous study [34] in participants with implanted depth electrodes. We first computed the power spectrum, using the BOSC method, for randomly selected (n = 100) 5 s-long iEEGs during trials (P_1). Power spectra were then computed for these iEEGs after they were filtered using the above-mentioned filter settings (P_2). A similarity index was computed between the two matrices (P_1 and P_2) using cosine distance defined as follows:

$$d_{ij} = \frac{p_{1i}\, p'_{2j}}{\sqrt{\left(p_{1i}p'_{1i}\right)\left(p_{2j}p'_{2j}\right)}}.$$

A similarity index was then calculated while allowing for the frequency lower bound to vary (Figure S4A). The same procedure was done on the similarity index calculated between the matrices consisting of data points with significant oscillations (Figure S4B).

Extraction of theta from iEEG

Raw signal was bandpass filtered (between 3–12 Hz) using an acausal 4th order Butterworth filter (Figure 2A). The phase and amplitude of theta was then computed from the filtered signal using Hilbert transform.

Statistics

Two-sided nonparametric Wilcoxon rank-sum test was utilized to assess the significant differences between linear variables. For each histogram, a kernel smoothing function was also computed for the probability density estimates. Values are expressed as median, [25th, 75th] or mean ± s.e.m when applicable. To control for familywise error rates, we used a method proposed by Maris and Oostenveld [32] that allows for multiple comparisons correction. In particular, when searching for frequency bins in which there were significant differences in oscillatory properties (p-episodes in Figure 4 and average duration of oscillatory bouts in Figure 6), the adjacent frequency bins cannot be assumed independent. Thus, the cluster-based permutation test performs 1000 permutations for an alpha level of 0.05 and finds clusters of significant data while accounting for multiple comparisons.

Classification of movement speed using machine learning

To classify behavior into fast and slow movement speeds (here referring to the top and bottom 30% of the running speeds respectively), we used a feed forward neural network with an input layer, a hidden layer consisting of 100 neurons and an output layer with a binary classifier (the corresponding speed categories). A tan-sigmoid function and a scaled conjugate gradient algorithm were used as a transfer function and back propagation algorithm respectively (Figure S5B). For each participant, the BOSC method was utilized to compute a power spectrum of the iEEG for each time point (Figure S5A). Data from all channels were concatenated (leaving a contiguous 15% of the total data out for the testing set to ensure independence). For the remaining data, 85% was used for training while the other 15% was used for cross validation. Receiver operating characteristic (ROC) plot and the area under that curve (AUC) were used to evaluate the performance of our model (Figure S5C).

DATA AND SOFTWARE AVAILABILITY

Data files, as well as the codes used in MATLAB and SPSS, are available from the Lead Contact upon reasonable request. Results presented in this manuscript were uploaded to the BioRxiv preprint server in September 2016 (http://biorxiv.org/content/early/2016/09/28/078055).

Current Biology, Volume *27*

Supplemental Information

Theta Oscillations in the Human Medial Temporal Lobe during Real-World Ambulatory Movement

Zahra M. Aghajan, Peter Schuette, Tony A. Fields, Michelle E. Tran, Sameed M. Siddiqui, Nicholas R. Hasulak, Thomas K. Tcheng, Dawn Eliashiv, Emily A. Mankin, John Stern, Itzhak Fried, and Nanthia Suthana

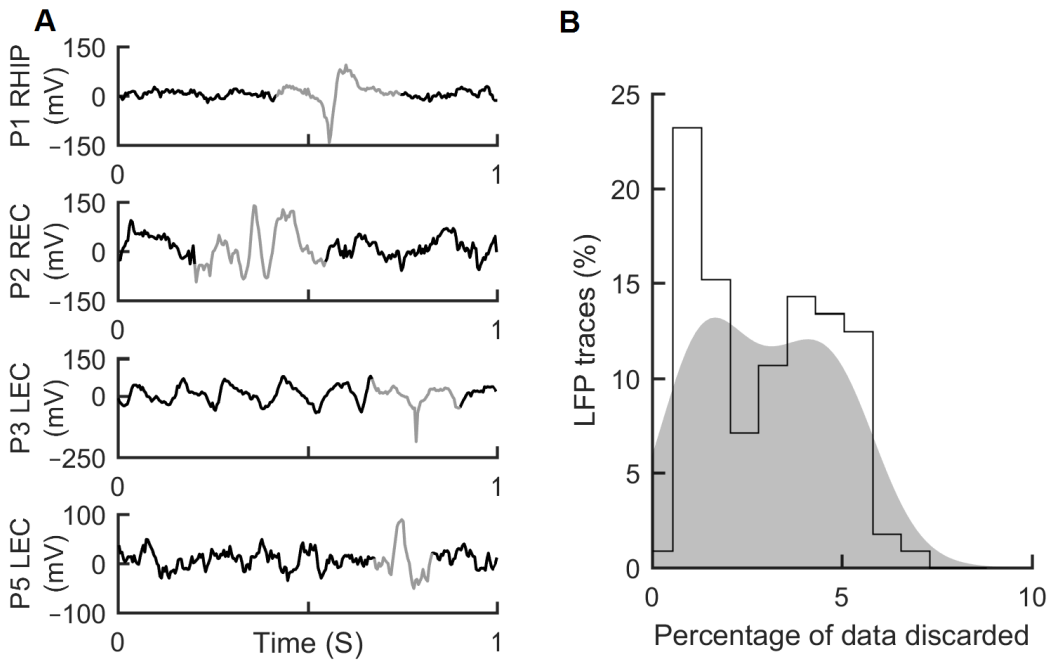

Figure S1. Elimination of epileptic discharges (related to Figure 2).

(A) Shown are example one-second-long iEEG traces from 4 different participants (in black) and epileptic discharges detected (in gray) using thresholding methods (see the STAR Methods). **(B)** Putative epileptic epochs were detected on iEEGs from all channels and within all trials, and data from these periods were discarded from analysis (percentage of epileptic epochs = 3.04, [1.32, 4.62]%, $N_{participants}$ = 4, $N_{trials \times channels}$ = 112). The percentage of putative epileptic data was similar during slow movements (3.08, [1.37, 4.41]%) and fast movements (3.01, [1.46, 5.01]%) and not significantly different from one another (p = 0.6, Wilcoxon rank-sum test). Numbers are reported as median, [25^{th}, 75^{th}]. Shaded area corresponds to kernel smoothing function estimate of the distribution.

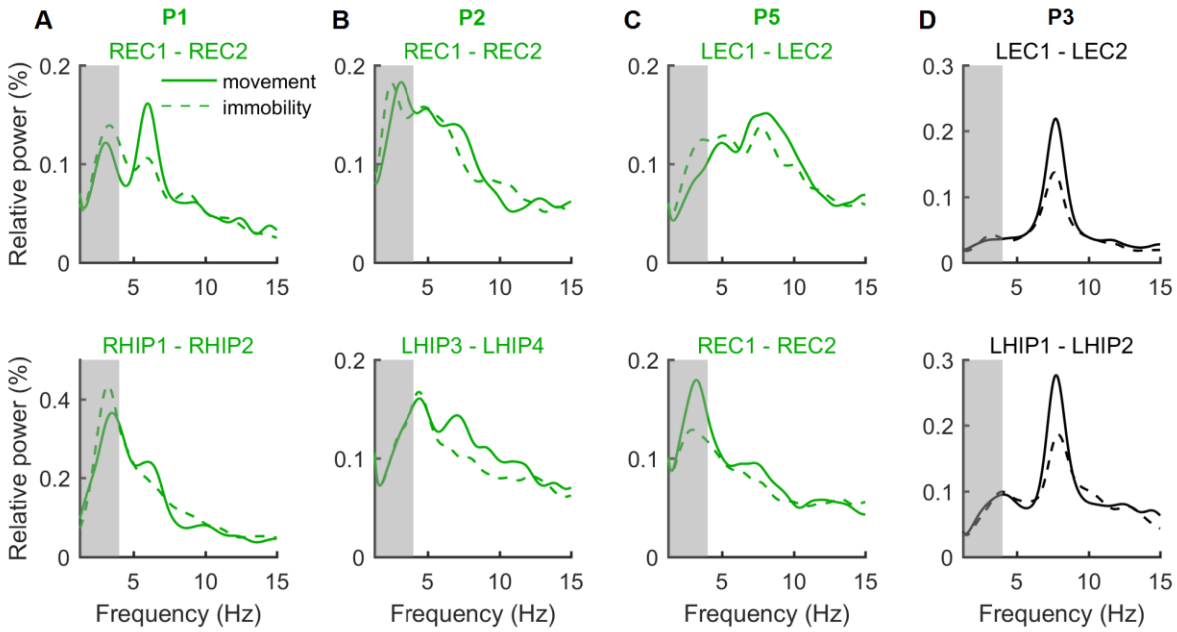

Figure S2: Example power spectra from individual participants (related to Figure 3). **(A-C)** Example (normalized) power spectra from sighted participants during movement (solid lines) and periods of immobility (dashed lines). Each column represents one participant and each row corresponds to one representative channel in the entorhinal cortex or the hippocampus region. The clinical channel names are noted at the top of each panel (for electrode localizations see Table S3). **(D)** Same as in **A-C** but in the congenitally blind participant. Values below 4 Hz (lower range of the analog bandpass filter) are marked with shaded gray areas.

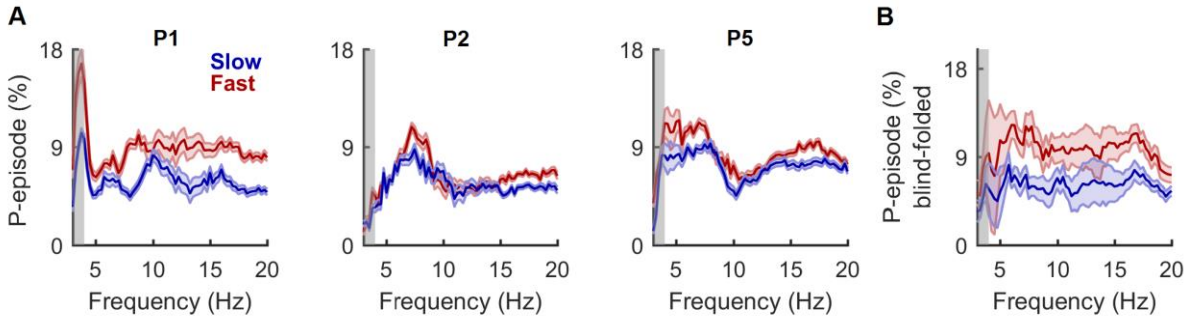

Figure S3. Increased prevalence of theta oscillations during fast versus slow movements within individual sighted participants, and when they are blindfolded (related to Figure 4).

(A) Analysis of p-episodes within each sighted participant exhibited qualitatively similar results to the overall results from all participants shown in Figure 4B. Namely, theta was more prevalent during fast (red) compared to slow (blue) movements. Shown are the mean ± SEM). **(B)** Two participants (P1 and P5) performed the task while being blindfolded (4 channels in each participant, $N_{total} = 8$). Within each trial, data were divided into slow and fast movement speeds—although movement speeds were overall slower due to blindfolding—and p-episodes were detected in each condition. The p-episodes with significant theta oscillations were comparable to those found under normal conditions (Figure 4B), demonstrating that blindfolding the sighted participants does not lead to the results found in the congenitally blind participant. Values below 4 Hz (lower range of the analog bandpass filter) are marked with shaded gray areas.

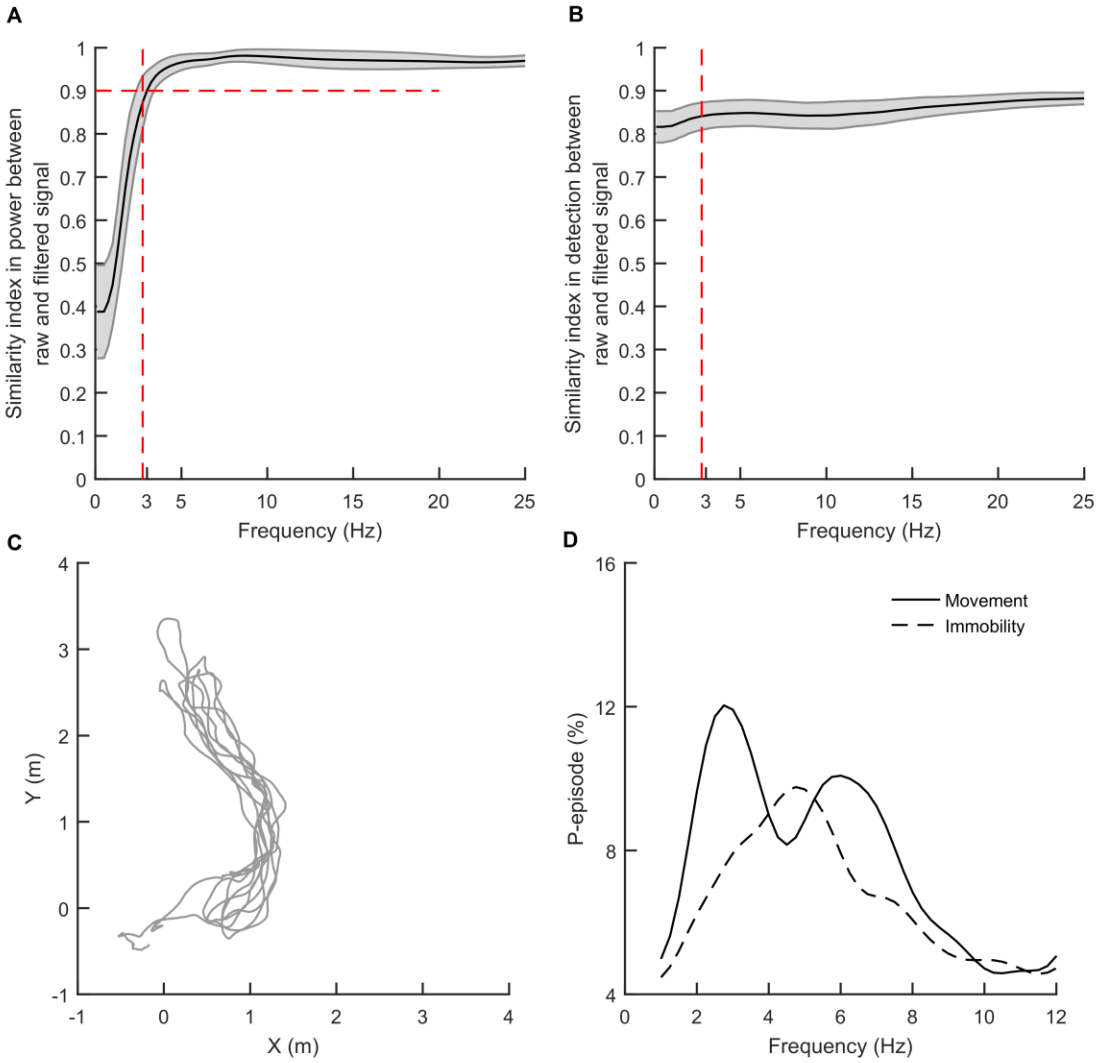

Figure S4. Control analyses for comparisons of oscillation detection patterns using raw wide-band signals recorded from depth subjects and signals recorded via the RNS® System (related to Figure 4).

We used data collected from a previous study [S1] in participants acutely implanted with intracranial depth electrodes for seizure monitoring. We mathematically implemented a filter, analogous to that existing on the RNS® System, on this wide-band data to investigate the effects of filtering on our oscillation detection algorithms. **(A)** Similarity index between power spectra computed using the BOSC method from the raw wide-band signal and bandpass filtered signal after the frequencies shown on x-axis (mean ± SEM, N_{trials} = 100, $n_{participants}$ = 2). Dashed red line indicates the frequency above which the similarity index is higher than 0.9 (F = 3 Hz). Thus, we used 3 Hz as the cutoff frequency below which our results cannot be interpreted. **(B)** Similarity index between the matrices consisting of significant oscillations detected in the raw and filtered signal. Above F = 3 Hz (our chosen cutoff frequency), this index was greater than 0.84. **(C)** Movement trajectory of a depth subject walking in the hospital room while movement was tracked using Google's Project Tango tablet. **(D)** Using the BOSC method, we quantified the percentage of time with significant oscillations (p-episodes) for periods of movement (solid line) and immobility (dashed line). Note that ~8 Hz theta oscillations are present during movement ~10% of the time, which is consistent with our findings in participants implanted with the RNS® System.

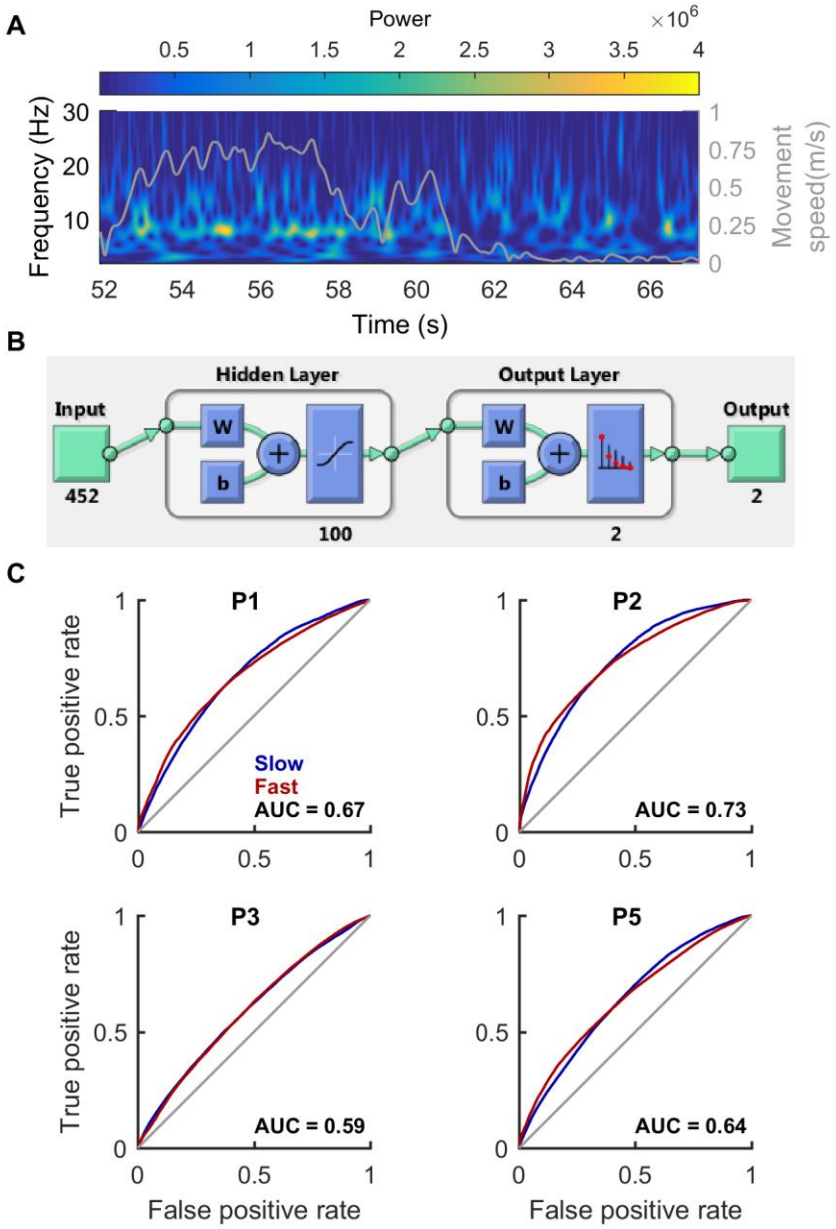

Figure S5. Neural networks as a tool to decode movement speeds (related to Figure 4).

(A) Power spectra were computed by convolving Morlet wavelets with the signal (the first analysis step in the BOSC method). An example power spectrum from a channel (the left hippocampus, CA1) is shown overlaid with the movement speed of the participant (gray trace). **(B)** The structure of the network utilized for speed classification consisting of 100 neurons in the hidden layer and two output classes corresponding to the slow and fast movement speeds. Input data consisted of power spectra in 3-30 Hz frequency band, computed using the BOSC method (see the STAR Methods), and concatenated across all 4 channels. Classification was done separately for each participant. **(C)** ROC plots from all participants showed that our model could successfully predict the two classes (fast speeds in red, slow speeds in blue) as indicated by the distance between the lines from the two classes and chance level (gray diagonal line). The area under the ROC curve (AUC), a measure commonly used to describe the performance of a classification model, for each participant is reported at the bottom right. Note that in all cases, AUC values are above 0.5 (the area under diagonal line or the chance level).

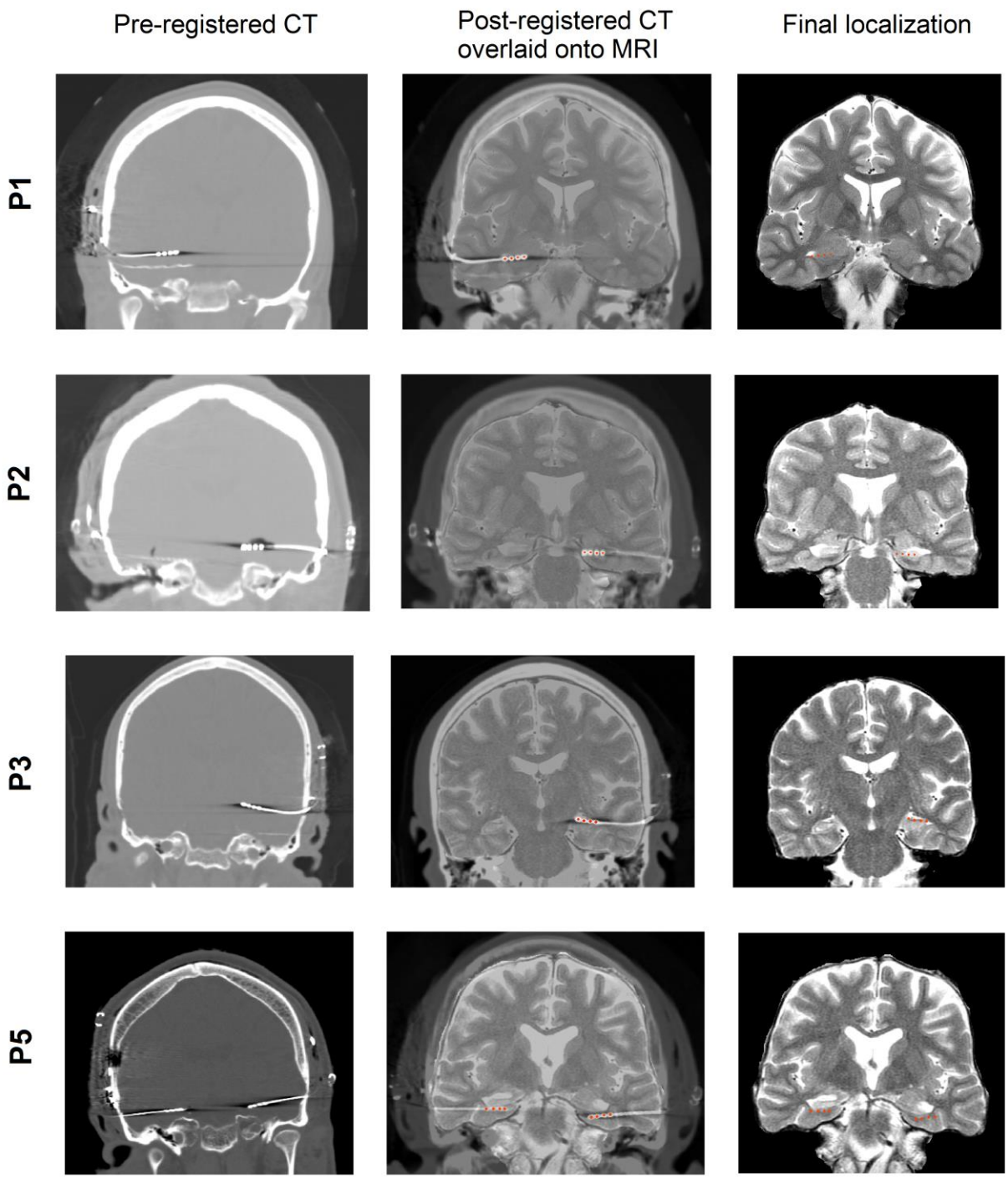

Figure S6. Map of individual pre- and post-registered CT images for all participants (related to Figure 2).

Subject	Age	Gender	Handedness
P1	34	F	R
P2	40	F	L
P3*	63	M	R
P4	40	F	R
P5	45	M	L

Table S1. Subject demographics (related to Figure 1).
Demographics of the study participants including age, gender and handedness. Data from participant P4 were excluded from analysis due to epileptic activity.
* Participant P3 is congenitally blind.

Subject No.	Verbal IQ	Digit Span	Verbal Memory		Visual Memory	Executive Function
			WMS	CVLT *Percentile*		
P1	113	10	66	79	34.5	91
P2	70	37	<1	<1	2	25
P3	108	14	73	84	-	84
P5	NA	16	<1	<1	<1	66

Table S2. Clinical characteristics of the study participants (related to Figure 1).
Each participant performed neuropsychological tests for clinical characteristics evaluation using methods described earlier [S1]. In brief, Wechsler Adult Intelligence Scale was used to calculate verbal and digit span. Verbal memory was assessed by the logical memory portion of the Wechsler Memory Scale (WMS) and the long-delay free-recall part of the California Verbal Learning Test (CVLT). Visual memory and executive function were tested using Rey-Osterrieth Complex Figure test and the Trail Making Test respectively. All measures are reported as percentiles with the exception of Verbal IQ reported as standardized scores.

Subject	Electrode labels	Electrode spacing	Localization	Seizure onset
P1	REC1	10 mm	Entorhinal Cortex	Right temporal
	REC2		Perirhinal Cortex	
	REC3		Fusiform Gyrus	
	REC4		Inferior Temporal	
	RHIP1	3.5 mm	CA1	
	RHIP2		CA1	
	RHIP3		CA1	
	RHIP4		CA1	
P2	REC1	3.5 mm	Entorhinal Cortex	Left temporal
	REC2		Perirhinal Cortex	
	REC3		Perirhinal Cortex	
	REC4		Fusiform Gyrus	
	LHIP1	3.5 mm	CA1	
	LHIP2		CA23DG	
	LHIP3		CA23DG	
	LHIP4		CA23DG	
P3	LEC1	10 mm	Entorhinal Cortex	Left temporal
	LEC2		Perirhinal Cortex	
	LEC3		Inferior Temporal	
	LEC4		Inferior Temporal	
	LHIP1	3.5 mm	CA1	
	LHIP2		CA1	
	LHIP3		CA1	
	LHIP4		CA1	
P5	LEC1	3.5 mm	Entorhinal Cortex	Left mesial temporal
	LEC2		Perirhinal Cortex	
	LEC3		Perirhinal Cortex	
	LEC4		Fusiform Gyrus	
	REC1	3.5 mm	Subiculum	
	REC2		Subiculum	
	REC3		CA1	
	REC4		Fusiform Gyrus	

Table S3. Electrode localizations (related to Figures 2, 3, 4).
Electrode labels were determined based on clinical criteria and include R(L)EC, corresponding to right (left) entorhinal cortex area, and R(L)HIP corresponding to right (left) hippocampus. The precise location of the clinical electrode labels is shown in column 4, and were determined using automated segmentation software coupled with visual inspection of images resulted from co-registration of high resolution CT and MRI images [S1] (Figure 2B, see the STAR Methods). Smaller digits in the electrode labels indicate more distal (deeper) contacts. Further, the recordings were bipolar using adjacent electrodes 1-2 and 3-4 (e.g., REC1-REC2 and REC3-REC4 are two example iEEG channels).

Supplemental References:

S1. Suthana, N.A., Parikshak, N.N., Ekstrom, A.D., Ison, M.J., Knowlton, B.J., Bookheimer, S.Y., and Fried, I. (2015). Specific responses of human hippocampal neurons are associated with better memory. Proc. Natl. Acad. Sci. *112*, 10503–10508.